Reliable Global Path Planning of Off-road Autonomous Ground Vehicles Under Uncertain Terrain Conditions

Jianhua Yin, *Member, IEEE*, Lingxi Li, *Senior Member, IEEE*, Zissimos P. Mourelatos, Yixuan Liu, David Gorsich, Amandeep Singh, Seth Tau, and Zhen Hu

***Abstract*—Path planning plays a vital role in ensuring the efficient and safe operation of off-road autonomous ground vehicles (AGVs). Current methods mostly focus on minimizing the travel time or path length of AGVs and often overlook the fact that the AGVs could fail in many ways during the operation due to stochastic and rough terrain conditions. The objective of this paper is to not only generate a proper path for the vehicle but also ensure that the planned path is overall reliable and safe for the vehicle with complex terrain conditions. To achieve this goal, this paper develops a reliability-based mission planning method for off-road AGVs subject to two failure modes in terms of mobility (the maximum attainable speed and vehicle vertical acceleration) induced by the uncertain ground properties of the terrain. A physics-based vehicle dynamics simulation model is first employed to predict vehicle mobility for any given terrain conditions of a path. Mobility reliability of an AGV is then analyzed using surrogate modeling methods considering uncertainty sources in the off-road terrain conditions. After that, the reliability constraints for the two failure modes are integrated with the Rapidly-exploring Random Tree Star (RRT*) algorithm to identify an optimal path, which is the shortest path while satisfying the reliability requirements of the two considered failure modes. Results of a case study demonstrated the effectiveness of the proposed methods for path planning with the consideration of uncertainty in the deformable terrain.**

***Index Terms*—Mission mobility reliability, path planning, surrogate modeling, RRT*.**

I. Introduction

OFF-ROAD autonomous ground vehicle (AGV) is gaining increased attention in recent years, due to their promising potential in replacing human in harsh and/or boring working environments [1]–[3], such as transportation of supplies to battlefield [4], exploration of outer space [5], and reducing human labor in agricultural industry [6]. Since an AGV operates autonomously in the off-road environment, mission/path planning [7]–[9] is of paramount importance in guaranteeing the successful operation of the AGVs. An effectively planned path can increase operational efficiency (by minimizing the travel length and time) and reduce the risk of failure of AGVs (via navigating the vehicles away from obstacles).

Motivated by optimizing the operation performance of AGVs, various mission/path planning methods have been developed in recent years. The current path planning methods can be roughly classified into two categories, namely, global path planning and local path planning. Global path planning [10]–[13] identifies a path for any given starting point and end point based on certain global map information of a region of interest. Local path planning [14]–[18] optimizes the route locally in real-time according to the surrounding information collected from AGV sensors, such as LiDAR, camera, etc.

While the current global and local path planning methods have shown promising performance for on-road robots and autonomous vehicles, their applications to off-road AGVs face major barriers for several reasons. First, the widely used sensing techniques for obstacle detection in local path planning may fail to detect the obstacles in the complex off-road environments. For instance, an off-road AGV may get stuck in the soil and becomes immobile due to the deformable terrain, such as sand, mud pond, and wet soil. Even if the vision-based detection method is able to detect that the terrain is mud or sand, it cannot tell if the vehicle will get stuck or not, purely based on the sensing techniques. In that case, the obstacle becomes undetectable for local path planning methods [19]. Second, the off-road environment is highly uncertain. Due to the uncertainty in the soil properties, the mobility of a vehicle is uncertain [20]. For a region with deformable terrain, the vehicle might pass or get stuck. It implies that the problem is probabilistic instead of deterministic. Both the current global and local path planning methods for off-road vehicles or robots lack the capability of addressing this challenging issue. Third, most of the current global path planning methods for on-road AGVs or robots focus on minimizing the travel distance or time. For off-road AGVs, however, there are many more factors beyond travel distance and time that need to be considered due to the unstructured operation environment and uncertainty sources in the terrain and soil maps.

Corresponding author: Zhen Hu.

Jianhua Yin, Yixuan Liu, and Zhen Hu are with the Department of Industrial and Manufacturing Systems Engineering, University of Michigan-Dearborn, Dearborn, MI 48128, USA. (E-mail: yin1991me@gmail.com, {yixuanli, zhennhu}@umich.edu)

Lingxi Li is with the Transportation and Autonomous Systems Institute (TASI), also with the Department of Electrical and Computer Engineering, Purdue School of Engineering and Technology, Indiana University-Purdue University Indianapolis (IUPUI), 723 West Michigan Street, SL-160, Indianapolis, IN 46202, USA. (E-mail: LL7@iupui.edu)

Zissimos P. Mourelatos is with the Mechanical Engineering Department, Oakland University, Rochester, MI 48309, USA. (E-mail: mourelat@oakland.edu)

David Gorsich, Amandeep Singh, and Seth Tau are with the U.S. Army Combat Capabilities Development Command, Ground Vehicle Systems Center, Warren, MI 48397, USA. (E-mail: {david.j.gorsich.civ, amandeep.singh2.civ, seth.a.tau.civ}@army.mil)

DISTRIBUTION A. Approved for public release; distribution unlimited. OPSEC #7092

Aiming to address the above challenges in the mission planning of off-road AGVs, significant efforts have been made in recent years [21], [22]. A key technique, in tackling the issue that obstacles sometimes are undetectable or the uncertainty in vehicle mobility, is the physics-based modeling and simulation (M&S) for vehicle mobility prediction. In the past decades, various mobility models have been proposed, including semi-empirical models and high-fidelity simulation models. Semi-empirical models are from the simplified physics represented by empirical equations and have a high computation efficiency. For example, the NATO Reference Mobility Model (NRMM) and its advanced version developed by the U.S. Army [23], [24]. These models either use the vehicle cone index to evaluate the mobility on different soils or predict vehicle mobility based on the mean maximum pressure [25]–[27]. Due to model simplifications and assumptions, the empirical models may have large errors in mobility prediction [28]. To address this limitation, efforts have been made in recent years to develop the next-generation NATO Reference Mobility Model (NG-NRMM) using high-fidelity multi-physics simulations [29], [30]. In parallel with the NG-NRMM effort, numerous simulation models have also been developed. For instance, Xia [31] developed a tire-terrain interaction model using the Finite Element Method (FEM) to predict tire mobility. A nonlinear multi-physics co-simulation model was proposed using FEM and discrete element method to capture the coupled vehicle-tire-terrain interactions and predict the vehicle mobility on granular material [32].

Based on the physics-based M&S of off-road AGVs, approaches have also been developed in recent years to deal with uncertainty in the mobility prediction model. For example, Gonzalez et al. [33] predicted the mobility considering uncertainty in terrain elevation using Kriging and Monto Carlo simulation. Choi et al. [34] developed a reliability-based stochastic mobility map using a dynamic Kriging method to predict the mobility of AGVs. Compared with the deterministic approach, it was shown that the stochastic approach improves the reliability of path planning. However, these methods overlooked the space-dependency of the environmental uncertainty [35], [36] that the AGVs encounter and cannot be used to quantitatively understand the effects of terrain and soil uncertainty on the results of path planning. To address this issue, Jiang et al. [19] and some following works [37], [38] proposed several reliability-based path planning methods taking space-dependent uncertainty into account [39]–[41].

Although different methods have been developed for path planning in the past decades, identifying a reliable and shortest path for off-road AGVs is still a very challenging problem. An AGV could fail in the off-road environment in many different ways, such as extreme acceleration, running out of power, overturning, to name a few. Different failure modes require different analysis and prediction approaches. Current reliability-based path planning methods, however, only consider mobility from the AGV speed perspective through a quantity called the speed-made-good which is a quasi-static response. In rough terrain conditions, the AGV also suffers from extreme vibration excitation. The rough terrain elevation could lead to extreme dynamics behavior of AGVs and thereby cause damage to the health of the components inside vehicles as well as vehicle structures. Therefore, it is ultimately necessary to consider the multi-dimensional mobility of AGVs in path planning under uncertain off-road environment.

With a focus on global path planning, the objective of this paper is to develop a reliability-based path planning method for off-road AGVs by considering uncertainty sources in the terrain conditions. In particular, two major failure modes, including the maximum attainable speed and maximum vertical acceleration, are investigated using physics-based modeling and simulation. Based on the reliability assessment, a reliability-based optimization model is formulated for path planning by integrating the rapidly-exploring random tress star (RRT*) with the reliability constraints. The main contributions of this paper can be summarized as follows:

- A reliability-based path planning method based on RRT* with considering two failure modes due to uncertain terrain conditions is proposed to ensure the success of the mission.
- To overcome the challenges in computational cost caused by the high-fidelity vehicle mobility simulation in reliability analysis, different surrogate models are constructed to efficiently predict different failure modes without sacrificing accuracy. Specifically, an adaptive surrogate modeling method is used for the prediction of vehicle mobility reliability with respect to the speed-made-good failure mode. A dynamic ensemble-based dynamic surrogate modeling method is adopted to efficiently predict vertical acceleration under rough terrain conditions.
- The efficiency of path planning with multiple reliability considerations is improved by minimizing the worst case. Since the incorporation of reliability constraints increases the required computational effort for path planning, minimizing the worst-case can avoid unnecessary reliability assessment, thereby reducing the computational effort.

The remainder of this paper is organized as follows. The background of this study is reviewed in Section II. In Section III, we present approaches for mobility reliability analysis with respect to different mobility failure modes. Based on that, Section IV discusses reliability-based path planning subject to two reliability constraints. A case study is used to demonstrate the proposed algorithms in Section V. Finally, conclusions and future work are provided in Section VI.

II. Background

A. M&S-Based Global Path Planning of Off-Road AGVs

Global path planning of off-road AGVs is to find the shortest path in a certain area from a start point to a target point while satisfying specific requirements. Physics-based M&S plays a critical role in predicting the mobility and global path planning of AGVs. As shown in Fig. 1, M&S-based global path planning of AGVs in general consists of four main steps, namely,

1) The terrain conditions in the target area are characterized using topographic information (height map) and soil information (soil map). The target area map could be obtained either from satellite or other sources.

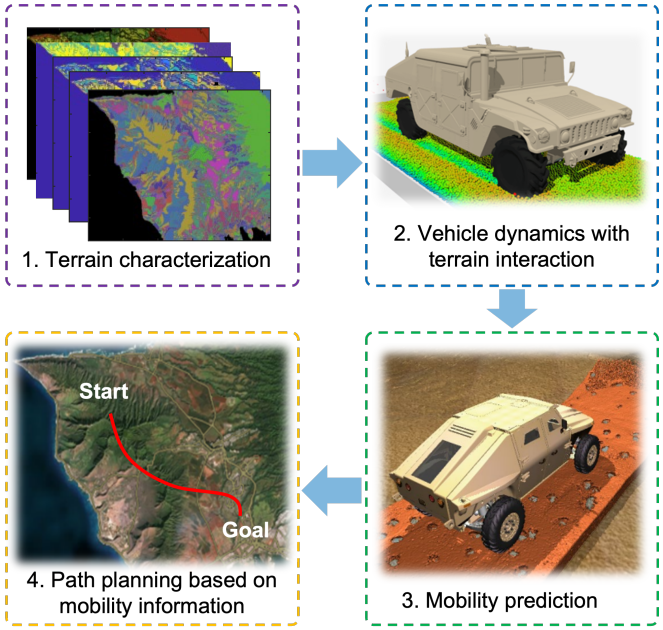

Fig. 1. Illustration of physics-based path planning for off-road autonomous ground vehicles.

2) The vehicle dynamics behavior is simulated considering the interaction between terrain conditions and the vehicle.
3) The vehicle mobility is predicted at arbitrary locations in the target area.
4) The results of mobility prediction are combined with path planning algorithms to find the optimal path with satisfying mobility requirements.

Several concepts are defined here and used for path planning. The target map is called a configuration space denoted by Ω. In the configuration space, the space with obstacles is called obstacle space, denoted by Ω_{ob}. The space that AGVs can fulfill the mission is called free space represented by Ω_{fr}. The arbitrary location in the configuration space has two dimensions and is given by $\mathbf{x} = (x_1, x_2)$. The start point is also called the initial point represented by $\mathbf{x}_{ini}$. The end point is the target to achieve, which is denoted by $\mathbf{x}_{tr}$. The connection between any arbitrary nodes is called an edge. The planned path of the mission is defined by Γ.

B. Physics-based M&S

The mobility of an AGV is highly related to the vehicle dynamics and terrain conditions as shown in Fig. 1. A generalized formulation for the mobility model is given by

$$\mathbf{Y}(\mathbf{x}) = M(\mathbf{V}, \mathbf{S}(\mathbf{x})), \mathbf{x} \in \Omega, \quad (1)$$

where $\mathbf{Y}(\cdot)$ is the output or quantities of interest representing the vehicle mobility at location $\mathbf{x}$, e.g., the maximum attainable speed and maximum vertical acceleration, $M(\cdot,\cdot)$ is the mobility model in general, which could be an empirical model or a simulation model, $\mathbf{V}$ is a vector of vehicle-related parameters, and $\mathbf{S}(\cdot) = [S_1(\mathbf{x}), S_2(\mathbf{x}), \ldots, S_n(\mathbf{x})]^{\mathrm{T}}$ is a vector representing the surrounding conditions of the vehicle (e.g., slope and soil parameters).

With the mobility model, M&S is combined with the path planning algorithm (RRT*) to identify the optimal path while satisfying physical constraints.

C. RRT*

RRT* finds the optimal path by iterations of a growing tree structure starting from $\mathbf{x}_{ini}$. A random node ($\mathbf{x}_{rand} \in \Omega$) is generated using a sampling strategy. If $\mathbf{x}_{rand} \in \Omega_{ob}$, $\mathbf{x}_{rand}$ is rejected. The sampling process continues until a random sample is in the free space; namely, $\mathbf{x}_{rand} \in \Omega_{fr}$. Then the nearest node ($\mathbf{x}_{nst}$) to $\mathbf{x}_{rand}$ in tree $\mathbf{T}$ is identified. If $\mathbf{x}_{rand}$ is accessible to $\mathbf{x}_{nst}$, meaning that there is no obstacle between $\mathbf{x}_{rand}$ and $\mathbf{x}_{nst}$, $\mathbf{x}_{rand}$ is inserted to the tree by connecting $\mathbf{x}_{nst}$ and $\mathbf{x}_{rand}$. Otherwise, a new node $\mathbf{x}_{new}$ is generated using a steering function and added to the tree by connecting it to $\mathbf{x}_{nst}$. A collision check is performed to ensure that there is no obstacle between $\mathbf{x}_{new}$ and $\mathbf{x}_{nst}$. After $\mathbf{x}_{new}$ passes the collision check, the rewiring operation is used to modify the tree [42]. The above operations are executed iteratively until the optimal path is found.

D. Challenges in Path Planning of Off-Road AGVs

Reliable path planning of off-road AGVs is challenging for various reasons. Three of them are addressed in this work. The first challenge is the highly uncertain working environment of AGVs, which leads to a variation of AGV mobility as shown in Fig. 2. In a certain region with deformable soil, an AGV could have a certain probability of either passing or getting stuck. Understanding the effect of uncertainty on mobility performance is critical for path planning of off-road AGVs.

Another challenge is that AGVs could lose mobility in another way, but current methods only consider mobility in terms of the speed of AGVs, called speed-made-good reliability. Except speed made good, a highly possible failure is the vehicle and supplies being damaged due to extreme vibration. Considering mobility reliability from different perspectives is critical to ensure the success of a mission.

The third challenge is the computational efficiency [43]. The semi-empirical model is very efficient, but with large prediction errors. On the other hand, the high-fidelity simulation model is accurate but takes a very long time to run. For path planning with reliability constraints, the constraint evaluation needs thousands of simulations. If the high-fidelity simulation model is used for M&S, it is computationally prohibitive [44]. Modeling methods with high efficiency and guaranteed accuracy are therefore needed for reliability-based path planning.

To address these challenges, this work develops a path planning method with two reliability constraints by considering uncertainty sources in the deformable terrain. An adaptive surrogate model and a dynamic ensemble-based dynamic surrogate modeling method are used to efficiently assess reliability from two different perspectives. The detailed methodology is provided in the next two sections.

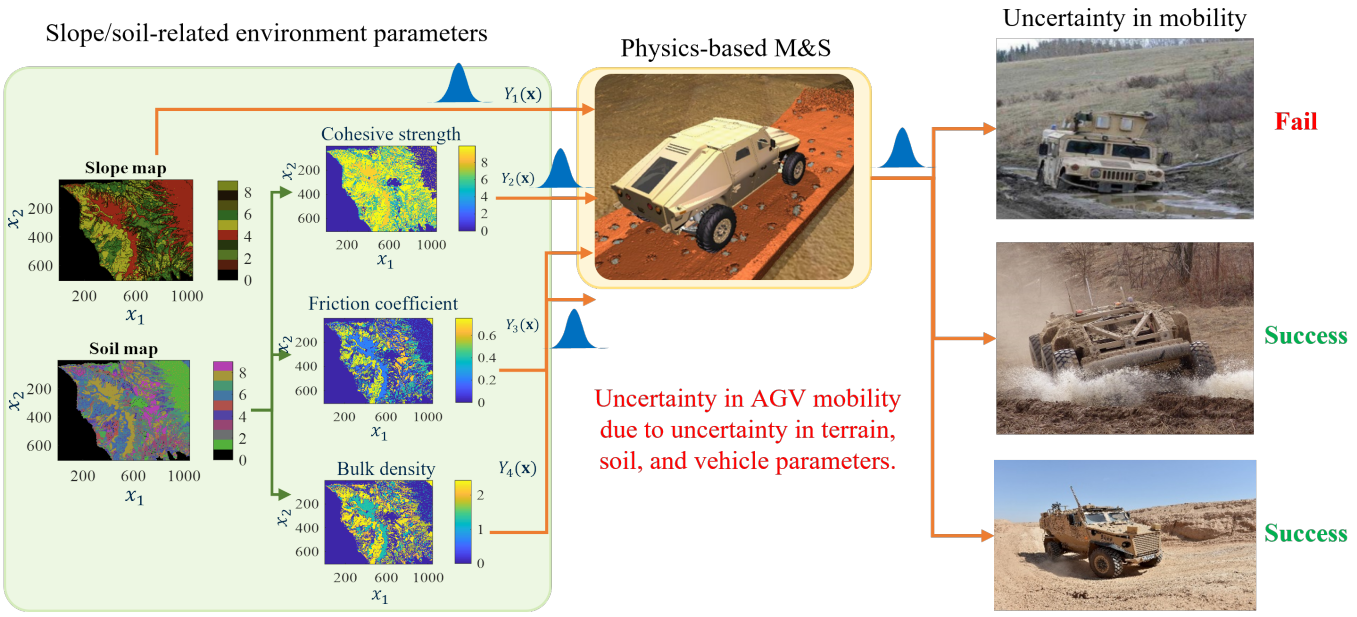

Fig. 2. Uncertainty sources and its impact on AGV mobility.

III. Multi-mode Reliability Analysis of Off-Road AGVs Subject to Uncertain Terrain Conditions

In this section, we first discuss how the uncertainty of terrain conditions are simulated, following are the detailed discussions of the two main failure modes of off-road AGVs induced by the uncertain terrain conditions.

A. Uncertainty sources and modeling

As discussed previously, without accounting for the prevalent uncertainty in path planning could lead to a high risk of failure of the off-road AGVs. Many failure modes could happen, such as vehicle getting stuck on a path (Fig. 2), vehicle overturning, running out of power, or goods damage due to severe vertical acceleration. In this paper, we focus on two main failure modes induced by uncertain terrain conditions, namely the maximum attainable speed and the maximum vertical acceleration. The uncertainty are from the terrain- and soil-related parameters, including the height of slope (h), soil properties such as Bekker coefficients (k_ϕ, k_c, B_n), soil cohesion (c), friction angle (ϕ_f), and Janosi shear displacement (J_s) [45]. Since the properties of these parameters are spatially correlated, we use Gaussian random field to simulate the parameter uncertainty.

The spatial correlation between any arbitrary two locations in the map is described by an auto-correlation function as

$$k_{12} = \exp\left\{-\left(\frac{\mathbf{x}_1 - \mathbf{x}_2}{\theta_{\mathbf{x}}}\right)^2\right\}, \tag{2}$$

where $\theta_{\mathbf{x}}$ is the correlation length along space; $\mathbf{x}_1$, $\mathbf{x}_2$ are two arbitrary points in the map, and k_{12} is the correlation between the two points.

In order to generate random realizations of the random fields for reliability analysis, the truncated Karhunen-Loeve (K-L) expansion [35] is employed as follows

$$R_f(\mathbf{x}) = \mu(\mathbf{x}) + \sum_{i=1}^{m} \sqrt{\lambda_i}\varphi_i(\mathbf{x})\xi_i, \tag{3}$$

where $R_f(\mathbf{x})$ is a generated realizations (samples) of a random field; $\mu(\mathbf{x})$ is the mean function in terms of the spatial coordinate $\mathbf{x}$ of the random field; m is the truncation number; λ_i and $\varphi_i(\mathbf{x})$ is the eigenvalue and eigenvector by performing eigen-analysis of the correlation matrix, respectively; and ξ_i, $i = 1, \cdots, m$ are independent standard Gaussian random variables.

In what follows, we explain the reliability analysis with respect to two failure modes by considering uncertainty sources in the terrain conditions.

B. Reliability Analysis for the Maximum Attainable Speed

In order to operate successfully in the off-road environment, an AGV needs to maintain a certain minimum speed to avoid getting stuck in the deformable terrain or for safety purpose in the battlefield. Based on this consideration, the reliability with respect to the maximum attainable speed is defined as

$$\mathrm{MMR}_v(\Gamma) = \Pr\{v_m(\mathbf{S}(\mathbf{x})) > v_e,\ \forall \mathbf{x} \in \Gamma\}, \tag{4}$$

where $v_m(\cdot)$ is the maximum attainable speed, v_e is a speed threshold, "$\forall$" stands for "for all", and $\mathbf{S}(\mathbf{x})$ is a vector of terrain- and soil-related parameters at the spatial location $\mathbf{x}$. The considered terrain- and soil-related parameters are $\mathbf{S}(\mathbf{x}) = (h(\mathbf{x}), k_\phi(\mathbf{x}), k_c(\mathbf{x}), B_n(\mathbf{x}), c(\mathbf{x}), \phi_f(\mathbf{x}), J_s(\mathbf{x}))$.

In this paper, the maximum attainable speed $v_m(\mathbf{S}(\mathbf{x}))$ for surrogate model construction is predicted using a high-fidelity simulation software called PyChrono [46], [47]. Fig. 3 presents

an example of the dynamic simulation of off-road AGV motion in PyChrono.

A direct way of evaluating Eq. (4) is to propagate the realizations of the random field through the PyChrono simulation model as illustrated in Fig. 2. However, such a direct Monte Carlo simulation (MCS) is computationally prohibitive. To address this challenge, an adaptive surrogate model is adopted. The adaptive surrogate modeling method has been proven that it can accurately find the failure boundary with high efficiency [48]. We first generate N initial training points by Latin Hypercube sampling denoted by $\mathbf{S} = [\mathbf{S}_1, \mathbf{S}_2, \ldots, \mathbf{S}_N]^{\mathrm{T}}$. Their responses are obtained from PyChrono as $v_m = [v_{m1}, v_{m2}, \ldots, v_{mN}]^{\mathrm{T}}$. Given the training data, an initial Gaussian Process model (GP) is obtained as

$$\hat{v}_m = f(\mathbf{S})^{\mathrm{T}} \boldsymbol{\beta} + \varepsilon(\mathbf{S}), \tag{5}$$

where $\hat{v}_m$ is the predicted maximum attainable speed by GP; $f(\cdot)$ and $\boldsymbol{\beta}$ are vectors representing basis functions and corresponding coefficients, respectively; and $\varepsilon(\cdot)$ is an error term. The prediction by GP is not a single value but a normal distribution; namely, $\hat{v}_m \sim N\left(\mu_v(\mathbf{S}), \sigma_v^2(\mathbf{S})\right)$, where μ_v is the mean prediction and σ_v is the standard deviation denoting the prediction uncertainty.

In addition to the training data, we also generate a group of input samples using MCS as $\mathbf{S}_{\mathrm{MCS}} = \left\{\mathbf{S}^i\right\}_1^{N_{\mathrm{MCS}}}$. The corresponding predicted responses from the initial GP are denoted as $\hat{v}_m^i \sim N\left(\mu_v^i(\mathbf{S}^i), \left(\sigma_v^i(\mathbf{S}^i)\right)^2\right)$. Based on the MCS samples, we then identify new training points for the refinement of the GP model given in Eq. (5) by using the following active learning function

$$U(\mathbf{S}^i) = \frac{\left|\mu_v^i(\mathbf{S}^i) - v_e\right|}{\sigma_v^i(\mathbf{S}^i)}, \; i = 1, \ldots, N_{\mathrm{MCS}}, \tag{6}$$

where $\mathbf{S}^i$ is a point from $\mathbf{S}_{\mathrm{MCS}}$; The value of $U(\mathbf{S}^i)$ indicates the probability of misclassification. A lower value of $U(\mathbf{S}^i)$ means a higher probability that the sample is misclassified. We therefore identify the samples of $\mathbf{S}_{\mathrm{MCS}}$ in the vicinity of the failure boundary with lower $U(\mathbf{S}^i)$ value, until all $U(\mathbf{S}^i)$ from $\mathbf{S}_{\mathrm{MCS}}$ are greater than 2; namely, $\min\left\{\mathbf{S}^i\right\}_1^{N_{\mathrm{MCS}}} \geq 2$. Then, the active learning converges, and we have 95% confidence that the samples are correctly classified.

The new training sample $\mathbf{S}^*$ at each iteration is identified by

$$\mathbf{S}^* = \arg\min\left\{U(\mathbf{S}^i)\right\}_1^{N_{\mathrm{MCS}}}. \tag{7}$$

The identified new training sample is added to the training set to refine the GP model at each iteration. After the algorithm converges, the safe and failure region of the AGV maximum attainable speed is identified. MCS can be used to obtain the vehicle mission mobility reliability in terms of the maximum attainable speed (i.e. Eq. (4)) as

$$\begin{aligned} \mathrm{MMR}_v(\Gamma) &\approx \frac{1}{N_{\mathrm{MCS}}} \sum_{i=1}^{N_{\mathrm{MCS}}} I_v, \\ &\begin{cases} I_v = 0, \text{ if } \min_{x \in \Gamma} e_v(\mathbf{x}) < 0 \\ I_v = 1, \text{ if } \min_{x \in \Gamma} e_v(\mathbf{x}) \geq 0 \end{cases}. \end{aligned} \tag{8}$$

Now we have the first reliability constraint (MMR_v). Next, we discuss the details of the second reliability constraint in terms of the vertical acceleration.

C. Reliability Analysis with Respect to Vertical Acceleration

A major difference between the maximum attainable speed and the vertical acceleration is that the former is only affected by the terrain and soil properties at a specific spatial location while the latter is dependent on not only the terrain and soil at the current location, but also that of previous locations that an AGV passes through. Because of this, a different

Fig. 3. An example of simulating movement of an AGV in off-road environment in PyChrono.

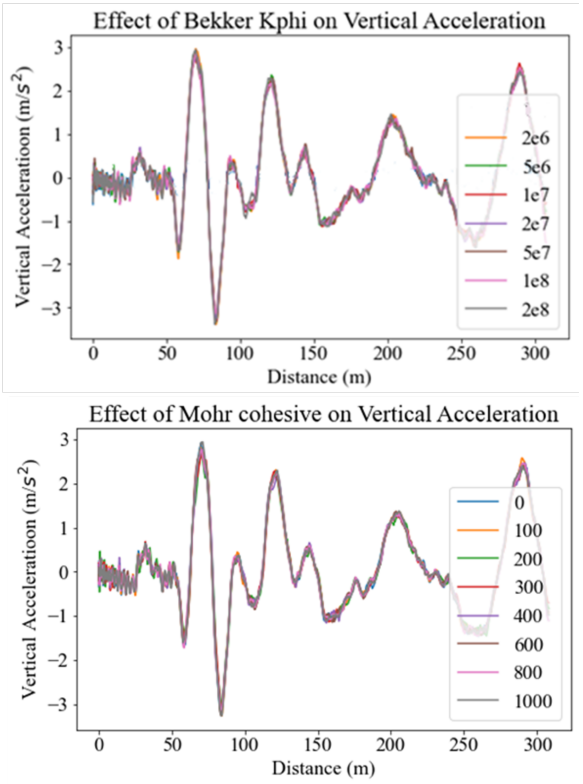

Fig. 4. Effects of soil parameters on the vertical acceleration.

reliability analysis method is required for the failure mode of the vertical acceleration. Moreover, from the results of PyChrono simulations, it is found that the vertical acceleration is insensitive to the soil parameters but closely related to the slope height. As shown in Fig. 4, given a path, different soils are used to simulate the vertical acceleration behavior along the path. It is shown that the soil type has a negligible impact on the vertical acceleration.

Hence, we can simplify the vertical acceleration model as a function of the terrain elevation as

$$a_i = f\left(h_i, h_{i-1}, \cdots, h_{i-p}; a_{i-1}, a_{i-2}, \cdots, a_{i-q}\right), \tag{9}$$

where a_i is the vertical acceleration at spatial location $\mathbf{x}_i$, $h_i = h(\mathbf{x}_i)$ is the elevation at $\mathbf{x}_i, \forall i = 1, \cdots, p$, and $f(\cdot)$ is a nonlinear function. This model is also called a Nonlinear Auto Regressive exogenous (NARX) model.

Due to the complicated off-road environment and the nonlinear vehicle dynamics, there is no analytical solution available for Eq. (9). In this section, we learn Eq. (9) using the synthetic mobility data collected from PyChrono simulations, and a recently developed dynamic ensemble of NARX Models (DENA) method is employed to accomplish this task [49]. The basic idea of DENA is first to train multiple NARX models with different segments divided from the whole prediction area using the Gaussian mixture model (GMM) [50]. Then, the NARX models are ensembled dynamically over paths to predict the vertical acceleration along the path.

More specifically, we first generate N_p paths for the off-road AGV. The heights (terrain elevation) of the N_p paths are denoted by h_j^i, $i = 1, 2 \ldots, N_p$, $j = 1, 2, \ldots, N_i$, where N_i is the number of coordinates for i-th path. Given the path information, the vertical acceleration is obtained by PyChrono simulation and is denoted by a_j^i, $i = 1, 2 \ldots, N_p$, $j = 1, 2, \ldots, N_i$. We then convert the data into the NARX format as

$$\mathbf{H}_T = \begin{bmatrix} \mathbf{h}^1 & \mathbf{a}^1 \\ \mathbf{h}^2 & \mathbf{a}^2 \\ \vdots & \vdots \\ \mathbf{h}^{N_T} & \mathbf{a}^{N_T} \end{bmatrix}, \tag{10}$$

where $\mathbf{H}_T$ is the training data from the paths generated; $\left\{\mathbf{h}^i \in \mathbb{R}^{1\times p}\right\}_1^{N_T}$ are heights from the segments of the paths with the length of p points; $\left\{\mathbf{a}^i \in \mathbb{R}^{1\times q}\right\}_1^{N_T}$ are the corresponding vertical acceleration from the same segments of the paths. Based on the first q points, we predict the next vertical acceleration $\left\{\mathbf{a}^{(q+1)i} \in \mathbb{R}^{1\times 1}\right\}_1^{N_T}$. We let $T = q+1$, then the corresponding prediction of the training points from Eq. (10) is given by

$$\mathbf{A}_T = \begin{bmatrix} a^{T1} \\ a^{T2} \\ \vdots \\ a^{TN_T} \end{bmatrix}. \tag{11}$$

Next, we partition all the training points and labels into different segments using Gaussian mixture model (GMM) to capture the dynamic behavior of AGVs in different dynamic regions. GMM approximates the join PDF of $\mathbf{H}_T$ as a weighted sum of multivariate Gaussian components as below

$$f\left(\mathbf{H}_T\right) = \sum_{k=1}^{Q} w_k \phi\left(\mathbf{H}_T \left| \boldsymbol{\mu}_k, \boldsymbol{\Sigma}_k \right.\right), \tag{12}$$

where Q is the number of Gaussian components; w_k is the weight of the k-th Gaussian component; $\boldsymbol{\mu}_k$ and $\boldsymbol{\Sigma}_k$ is the mean vector and the covariance matrix of the multivariate Gaussian distribution, respectively; and $\phi(\cdot)$ is the PDF of the multivariate Gaussian distribution.

After that, the probability that the i-th ($j = 1, \ldots, N_T$) training point belongs to k-th ($k = 1, \ldots, Q$) cluster is given by

$$p_k\left(\mathbf{H}_{T,i}\right) = P\left(\mathbf{H}_{T,i}, k \left| w_k, \boldsymbol{\mu}_k, \boldsymbol{\Sigma}_k \right.\right), \tag{13}$$

where $\mathbf{H}_{T,i}$ represent the i-th ($j = 1, \ldots, N_T$) training point in $\mathbf{H}_T$; $p_k\left(\mathbf{H}_{T,i}\right)$ denotes the probability that the training point belongs to the k-th ($k = 1, \ldots, Q$) cluster; and w_k, $\boldsymbol{\mu}_k$, $\boldsymbol{\Sigma}_k$ are the learned parameters from GMM. The summation of the probability $p_k\left(\mathbf{H}_{T,i}\right)$, $k = 1, \ldots, Q$ is 1 as

$$\sum_{k=1}^{Q} P\left(\mathbf{H}_{T,i}, k \left| w_k, \boldsymbol{\mu}_k, \boldsymbol{\Sigma}_k \right.\right) = 1. \tag{14}$$

Now we can divide the whole training points $\mathbf{H}_T$ into Q groups. Each of the group is denoted by

$$\mathbf{H}_{g,k} = \left\{\mathbf{H} \left| I_c\left(\mathbf{H}_{T,i}, k\right) = 1,\ \forall \mathbf{H} \in \mathbf{H}_T \right.\right\},\ k = 1, \ldots, Q. \tag{15}$$

Similarly, the corresponding predicted vertical accelerations in Eq. (11) are divided into the same Q groups, which is denoted by

$$\mathbf{A}_{g,k} = \left\{\mathbf{A} \left| I_c\left(\mathbf{A}_{T,i}, k\right) = 1,\ \forall \mathbf{A} \in \mathbf{A}_T \right.\right\},\ k = 1, \ldots, Q. \tag{16}$$

It is noted that a sample $\mathbf{H}$ and the corresponding $\mathbf{A}$ could belong to multiple groups, which means the training points of multiple NARX models could overlap. The samples and corresponding labels of each group are a subset of $\mathbf{H}_T$ and $\mathbf{A}_T$, respectively. The union of all subsets are $\mathbf{H}_T$ and $\mathbf{A}_T$, which is denoted by

$$\mathbf{H}_T = \left\{\mathbf{H}_{g,1} \cup \cdots \cup \mathbf{H}_{g,Q}\right\}, \tag{17}$$

$$\mathbf{A}_T = \left\{\mathbf{A}_{g,1} \cup \cdots \cup \mathbf{A}_{g,Q}\right\}. \tag{18}$$

Recall that every subset of training points is used to build a NARX model. Each NARX model is denoted by

$$\hat{a}_k = \hat{g}_{NX,k}\left(\mathbf{h}, \mathbf{a}\right),\ k = 1, 2, \ldots, Q, \tag{19}$$

where $\mathbf{h} = [h_d, h_{d-1}, \ldots, h_{d-q}]$ and $\mathbf{a} = [a_{d-1}, a_{d-2}, \ldots, a_{d-q}]$ represent the height and vertical acceleration first $q+1$ and q steps, respectively; $\hat{g}_{NX,k}(\cdot)$ denotes the NARX model; and $\hat{a}_k$ is the prediction at coordinate d by k-th NARX mdoel. In this paper, the GPR model is employed to learn $\hat{g}_{NX,k}(\cdot)$ based on data.

After all the NARX models are available, we assemble them dynamically over prediction length to predict the vertical

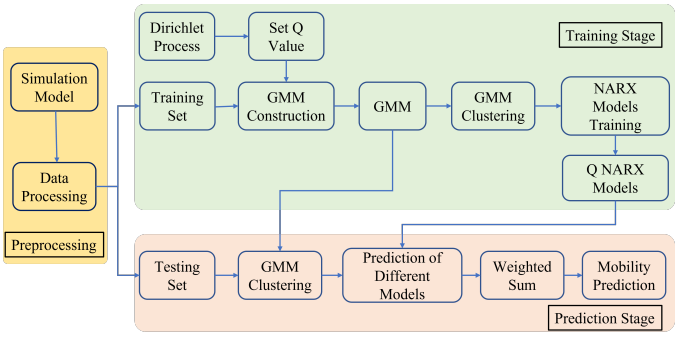

Fig. 5. Flowchart of Dynamic Ensemble of NARX model (DENA).

acceleration in a given path. The prediction at d coordinate by assembled DENA model is given by [49]

$$\hat{a}\left(d\right)=\sum_{k=1}^{Q}w\left(\mathbf{H}_{T,d},k\right)\hat{g}_{NX,k}\left(\mathbf{h},\mathbf{a}\right), \tag{20}$$

where $w\left(\mathbf{H}_{T,d},k\right)$ is denoted by

$$w\left(\mathbf{H}_{T,d},k\right)=\frac{\hat{p}_k\left(\mathbf{H}_{T,d}\right)}{\sum_{k=1}^{Q}\hat{p}_k\left(\mathbf{H}_{T,d}\right)}, \tag{21}$$

in which $\hat{p}_k\left(\mathbf{H}_{T,d}\right)$ is obtained by

$$\hat{p}_k\left(\mathbf{H}_{T,d}\right)=\begin{cases}p_k\left(\mathbf{H}_{T,d}\right), & \text{if } p_k\left(\mathbf{H}_{T,d}\right)\geq\frac{0.05}{Q-1}\\ 0, & \text{otherwise}\end{cases} \tag{22}$$

where $p_k\left(\mathbf{H}_{T,d}\right)$ is solved by Eq. (13) using GMM.

Since Gaussian Process regression is used to fit the dynamic behavior, we have $\hat{a}_k$ in Eq. (19) following a normal distribution as given below.

$$\hat{a}_k\sim N\left(\mu_{\hat{a}_k},\sigma^2_{\hat{a}_k}\right), \tag{23}$$

where $\mu_{\hat{a}_k}$ and $\sigma_{\hat{a}_k}$ are the mean and standard deviation of $\hat{a}_k$. By substituting Eq. (23) into Eq. (20), we have the mean prediction and standard deviation of DENA as shown below.

$$\mu_{\hat{a}}\left(d\right)=\sum_{k=1}^{Q}w\left(\mathbf{H}_{T,d},k\right)\mu_{\hat{a}_k}\left(\mathbf{h},\mathbf{a}\right), \tag{24}$$

$$\sigma_{\hat{a}}\left(d\right)=\sqrt{\sum_{k=1}^{Q}w^2\left(\mathbf{H}_{T,d},k\right)\sigma^2_{\hat{a}_k}\left(\mathbf{h},\mathbf{a}\right)}. \tag{25}$$

Once we have the DENA model constructed, the vertical acceleration along any given path can be predicted recursively. Fig. 5 summarizes the overall flowchart of DENA for off-road AGV vertical acceleration prediction.

As discussed previously, the severe vibration could cause damage to the goods and supply inside the AGV as well as some components of the AGV. Therefore, we set a threshold for vertical acceleration. Once the vertical acceleration along the path exceeds the threshold, the mission is assumed to be failed. Mathematically, we have,

$$I_a=\begin{cases}1, & \text{if } \max_{\mathbf{x}\in\Gamma}\hat{a}\left(\mathbf{x}\right)\leq a_{th}\\ 0, & \text{if } \max_{\mathbf{x}\in\Gamma}\hat{a}\left(\mathbf{x}\right)>a_{th}\end{cases}, \tag{26}$$

where $\hat{a}\left(\mathbf{x}\right)$ is the predicted acceleration by DENA along the planned path; a_{th} is the threshold vertical acceleration.

The reliability in terms of vertical acceleration by MCS is then computed by

$$\mathrm{MMR}_a\left(\Gamma\right)\approx\frac{1}{N_{\mathrm{MCS}}}\sum_{i=1}^{N_{\mathrm{MCS}}}I_a. \tag{27}$$

Next, we discuss how to integrate the above presented reliability constraints with the RRT* algorithm for reliability-based path planning of off-road AGVs.

IV. Path Planning Subject to Two Terrain-Related Reliability Constraints

A. Overview

Fig. 6 shows an overview of the proposed framework. As shown in this figure, the proposed framework consists of three main modules. The *first* and the *second* module focuses on mobility reliability analysis of off-road AGVs with respect to the maximum attainable speed and the maximum vertical acceleration, respectively. The *third* module integrates the reliability constraints into RRT*-based path planning algorithm to identify the path that is the shortest and satisfies the two reliability constraints.

To account for these two failure modes in path planning of off-road AGVs, the reliability-based path planning model is formulated as:

$$\begin{aligned}&\min C(\Gamma)\\ &\text{s.t.}\\ &\mathrm{MMR}_v\left(\Gamma\right)\geq R_v\\ &\mathrm{MMR}_a\left(\Gamma\right)\geq R_a\\ &\Gamma\in\Omega_{\mathrm{fr}},\end{aligned} \tag{28}$$

where Γ is the designed path; $C\left(\Gamma\right)$ is the cost in terms of Γ to minimize; $\mathrm{MMR}_v\left(\cdot\right)$ and $\mathrm{MMR}_a\left(\cdot\right)$ represents the mission mobility reliability in terms of the maximum attainable speed and the vertical acceleration, respectively.

Next, we discuss how to integrate the reliability constraints into the RRT* algorithm for path planning. We name the proposed method as TRs-RRT*, which means RRT* with reliability constraints considering the uncertainty of deformable terrain.

B. TRs-RRT*

As discussed in Sec. II-C, we first initialize a tree denoted by $\mathbf{T}$ which contains all the nodes generated during the path exploration. For the first step, only the start point $\mathbf{x}_{ini}$ and the target $\mathbf{x}_{tr}$ are in $\mathbf{T}$. Next, we randomly generate a node $\mathbf{x}_{rand}\in\Omega_{fr}$ and find the nearest node ($\mathbf{x}_{nst}$) in the tree to $\mathbf{x}_{rand}$. It is noted for the first random node, the nearest node is $\mathbf{x}_{ini}$. The function used to find the nearest node is given by

$$\mathbf{x}_{\mathrm{nst}}=\mathrm{Nearest}\left(\mathbf{T},\mathbf{x}_{\mathrm{rand}}\right)=\arg\min_{\forall\mathbf{x}\in\mathbf{T}}\left\|\mathbf{x}_{\mathrm{rand}}-\mathbf{x}\right\|. \tag{29}$$

After the random node is found, a steering function is used to generate a new node $\mathbf{x}_{new}$, which is denoted by

$$\mathbf{x}_{new}=\mathrm{steer}\left(\mathbf{x}_{rand},\mathbf{x}_{nst}\right), \tag{30}$$

where $\mathrm{steer}\left(\cdot\right)$ denotes the steering function. Then, the reliability MMR_v and MMR_a in Eqs. (8) and (27) from $\mathbf{x}_{ini}$ to

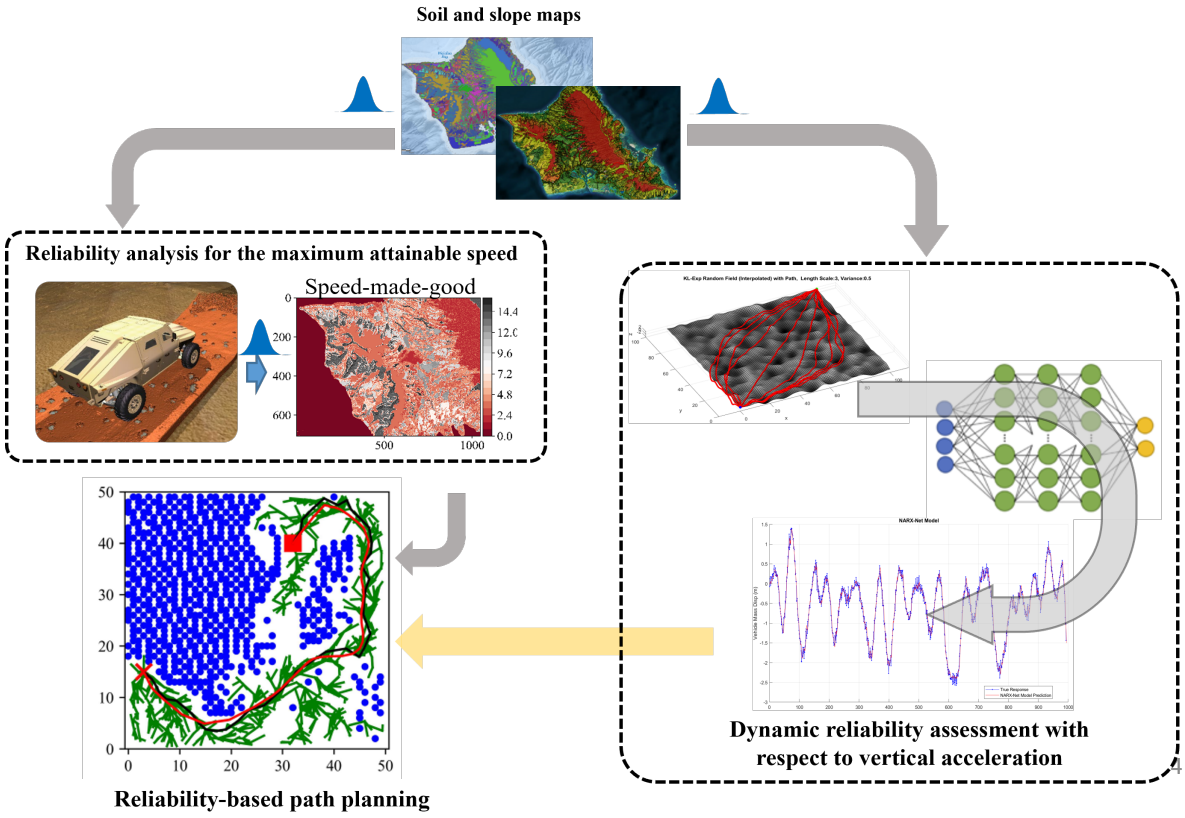

Fig. 6. Path planning subject to two terrain-related reliability constraints.

$\mathbf{x}_{new}$ are checked. If the path satisfies the reliability targets, the neighbor nodes within a radius are found and denoted by

$$\mathbf{X}_{nbor} = \mathrm{Near}\left(\mathbf{T}, \mathbf{x}_{new}\right). \tag{31}$$

The radius is defined by

$$r = \gamma \left(\frac{\log \vartheta}{\vartheta}\right)^{\frac{1}{dim}}, \tag{32}$$

where γ is a constant defined according to the environment, ϑ is the number of iterations, and dim is the dimension of configuration space.

After that, the best parent node for $\mathbf{x}_{new}$ is chosen from $\mathbf{X}_{nbor}$ with the lowest cost. The algorithm performs rewiring to rebuild the path to $\mathbf{x}_{new}$. The above operations execute iteratively until $\mathbf{x}_{new}$ arrives the region of the target point. The detailed TRs-RRT* is provided in Algorithm 1.

C. TRs-B-RRT*

To further improve the efficiency of TRs-RRT*, we propose the second algorithm called TRs-B-RRT* (where 'B' means binary operation) by using the GO/NO-GO map. The idea is to reduce the search domain for path planning before reliability analysis. As shown in Fig. 8, for the same location, the slope angle of the AGV passed depends on the orientations. Different orientations could result in different slope angles. For the same slope, the AGV could lose mobility in specific moving directions. Therefore, we use the worst case (the maximum slope) in predicting the maximum attainable speed. A binary operation based on the worset case is used to divide the configuration space into feasible and infeasible area. The min-max approach also could provide higher robustness for path planning.

In this case, we simply use the maximum slope to replace the slope information in Eq. (5) in predicting the mobility in terms of maximum attainable speed as below

$$\begin{aligned} e_{v,wrst} &= \hat{v}_{m,wrst} - v_{th} \\ &= f\left(s_{max}, \bar{\mathbf{S}}\right)^{\mathrm{T}} \boldsymbol{\beta} + \varepsilon\left(s_{max}, \bar{\mathbf{S}}\right) - v_{th}, \end{aligned} \tag{33}$$

where s_{max} is the maximum slope; $\bar{\mathbf{S}}$ represents the other parameters in $\mathbf{S}$ in Eq. (5), thereby, $\mathbf{S} = [s_{max}, \bar{\mathbf{S}}]$. Using state mobility reliability (SMR) [19], we have the GO/NO-GO map as follows.

$$\Omega_{\mathrm{GO}} = \left\{\mathbf{x} \in \Omega \,|\mathrm{SMR}_v\left(\mathbf{x}\right) \geq R_v\right\}, \tag{34}$$

$$\Omega_{\mathrm{NO-GO}} = \left\{\mathbf{x} \in \Omega \,|\mathrm{SMR}_v\left(\mathbf{x}\right) < R_v\right\}, \tag{35}$$

where Ω_{GO} and $\Omega_{\mathrm{NO-GO}}$ denote the feasible and infeasible area in map, respectively, R_v is the reliability target in terms of maximum attainable speed, and SMR_v is obtained using MCS as

$$\begin{aligned} &\mathrm{SMR}_v(\Omega) \approx \frac{1}{N_{\mathrm{MCS}}} \sum_{i=1}^{N_{\mathrm{MCS}}} I_{v,\mathrm{wrst}}, \\ &\begin{cases} I_{v,\mathrm{wrst}} = 0, \text{if } \min_{x\in\Omega} e_{v,\mathrm{wrst}}(\mathbf{x}) < 0 \\ I_{v,\mathrm{wrst}} = 1, \text{if } \min_{x\in\Omega} e_{v,\mathrm{wrst}}(\mathbf{x}) \geq 0 \end{cases}. \end{aligned} \tag{36}$$

Algorithm 1: TRs-RRT*

Data: R_v, R_a, $\mathbf{x}_{ini}$, $\mathbf{x}_{tr}$, h, $\mathbf{S}$;
Initialize: $\mathbf{N} \leftarrow \text{InitializeNodes}(x_{ini})$,
$\mathbf{E} \leftarrow \text{InitializeEdge}(\emptyset)$, $\mathbf{T} \leftarrow (\mathbf{N}, \mathbf{E})$,
$i = 1$;
Result: $\mathbf{T} = (\mathbf{N}, \mathbf{E})$, Γ;
for $i \leq N_{iter}$ **do**
  $i = i + 1$;
  $\mathbf{x}_{rand} \leftarrow \text{SampleFree}$;
  $\mathbf{x}_{nst} \leftarrow \text{Nearest}\,(\mathbf{T},\ \mathbf{x}_{rand})$;
  $\mathbf{x}_{new} \leftarrow \text{steer}\,(\mathbf{x}_{rand}, \mathbf{x}_{nst})$;
  if $\text{MMR}_v\,(\mathbf{x}_{new}, \mathbf{x}_{ini}, h, \mathbf{S}) > R_v$ &
   $\text{MMR}_a\,(\mathbf{x}_{new}, \mathbf{x}_{ini}, h, \mathbf{S}) > R_a$ **then**
    $\mathbf{X}_{nbor} \leftarrow \text{Near}\,(\mathbf{T}, \mathbf{x}_{new})$;
    $\mathbf{x}_{parent} \leftarrow \mathbf{X}_{nbor}$;
    $c_{min} \leftarrow Cost\,(\mathbf{x}_{ini}, \mathbf{x}_{parent}, \mathbf{x}_{new})$;
    foreach $\mathbf{x}$ in $\mathbf{X}_{nbor}$ **do**
      if $\text{MMR}_v\,(\mathbf{x}_{new}, \mathbf{x}_{ini}, h, \mathbf{S}) > R_v$ &
       $\text{MMR}_a\,(\mathbf{x}_{new}, \mathbf{x}_{ini}, h) > R_a$ &
       $Cost\,(\mathbf{x}_{ini}, \mathbf{x}, \mathbf{x}_{new}) < c_{min}$ **then**
        $\mathbf{x}_{parent} \leftarrow \mathbf{x}$;
        $c_{min} \leftarrow Cost\,(\mathbf{x}_{ini}, \mathbf{x}, \mathbf{x}_{new})$;
      else
        break;
      end
    end
    $\mathbf{N} \leftarrow \mathbf{N} \cup \mathbf{x}_{new}$, $\mathbf{E} \leftarrow \mathbf{E} \cup (\mathbf{x}_{new}, \mathbf{x}_{parent})$;
    foreach $\mathbf{x}$ in $\mathbf{X}_{nbor}$ **do**
      $c_{nbor} \leftarrow Cost\,(\mathbf{x}_{ini}, \mathbf{x}_{parent}, \mathbf{x})$;
      if $\text{MMR}_v\,(\mathbf{x}_{new}, \mathbf{x}_{ini}, h,\ \mathbf{S}) > R_v$ &
       $\text{MMR}_a\,(\mathbf{x}_{new}, \mathbf{x}_{ini}, h) > R_a$ &
       $Cost\,(\mathbf{x}_{ini}, \mathbf{x}, \mathbf{x}_{new}) < c_{nbor}$ **then**
        $c_{nbor} \leftarrow Cost\,(\mathbf{x}_{ini}, \mathbf{x}, \mathbf{x}_{new})$;
      else
        break;
      end
    end
    $\mathbf{E} \leftarrow (\mathbf{E} \setminus \{(\mathbf{x}, \mathbf{x}_{parent})\}) \cup \{(\mathbf{x}_{new}, \mathbf{x})\}$;
  else
    break;
  end
end

Algorithm 2: TRs-B-RRT*

Data: R_v, R_a, $\mathbf{x}_{ini}$, $\mathbf{x}_{tr}$, h, $\mathbf{S}$;
Initialize: $\mathbf{N} \leftarrow \text{InitializeNodes}(x_{ini})$,
$\mathbf{E} \leftarrow \text{InitializeEdge}(\emptyset)$, $\mathbf{T} \leftarrow (\mathbf{N}, \mathbf{E})$,
$i = 1$;
Result: $\mathbf{T} = (\mathbf{N}, \mathbf{E})$, Γ;
for $i \leq N_{iter}$ **do**
  $i = i + 1$;
  $\mathbf{x}_{rand} \leftarrow \text{SampleFree}$;
  $\mathbf{x}_{nst} \leftarrow \text{Nearest}\,(\mathbf{T},\ \mathbf{x}_{rand})$;
  $\mathbf{x}_{new} \leftarrow \text{steer}\,(\mathbf{x}_{rand}, \mathbf{x}_{nst})$;
  if $\text{obstacleFree}(\mathbf{x}_{nst}, \mathbf{x}_{new})$ &
   $\text{MMR}_v\,(\mathbf{x}_{new}, \mathbf{x}_{ini}, h, \mathbf{S}) > R_v$ &
   $\text{MMR}_a\,(\mathbf{x}_{new}, \mathbf{x}_{ini}, h, \mathbf{S}) > R_a$ **then**
    $\mathbf{X}_{nbor} \leftarrow \text{Near}\,(\mathbf{T}, \mathbf{x}_{new})$;
    $\mathbf{x}_{parent} \leftarrow \mathbf{X}_{nbor}$;
    $c_{min} \leftarrow Cost\,(\mathbf{x}_{ini}, \mathbf{x}_{parent}, \mathbf{x}_{new})$;
    foreach $\mathbf{x}$ in $\mathbf{X}_{nbor}$ **do**
      if $\text{obstacleFree}(\mathbf{x}, \mathbf{x}_{new})$ &
       $\text{MMR}_v\,(\mathbf{x}_{new}, \mathbf{x}_{ini}, h, \mathbf{S}) > R_v$ &
       $\text{MMR}_a\,(\mathbf{x}_{new}, \mathbf{x}_{ini}, h) > R_a$ &
       $Cost\,(\mathbf{x}_{ini}, \mathbf{x}, \mathbf{x}_{new}) < c_{min}$ **then**
        $\mathbf{x}_{parent} \leftarrow \mathbf{x}$;
        $c_{min} \leftarrow Cost\,(\mathbf{x}_{ini}, \mathbf{x}, \mathbf{x}_{new})$;
      else
        break;
      end
    end
    $\mathbf{N} \leftarrow \mathbf{N} \cup \mathbf{x}_{new}$, $\mathbf{E} \leftarrow \mathbf{E} \cup (\mathbf{x}_{new}, \mathbf{x}_{parent})$;
    foreach $\mathbf{x}$ in $\mathbf{X}_{nbor}$ **do**
      $c_{nbor} \leftarrow Cost\,(\mathbf{x}_{ini}, \mathbf{x}_{parent}, \mathbf{x})$;
      if $\text{obstacleFree}(\mathbf{x}, \mathbf{x}_{new})$ &
       $\text{MMR}_v\,(\mathbf{x}_{new}, \mathbf{x}_{ini}, h,\ \mathbf{S}) > R_v$ &
       $\text{MMR}_a\,(\mathbf{x}_{new}, \mathbf{x}_{ini}, h) > R_a$ &
       $Cost\,(\mathbf{x}_{ini}, \mathbf{x}, \mathbf{x}_{new}) < c_{nbor}$ **then**
        $c_{nbor} \leftarrow Cost\,(\mathbf{x}_{ini}, \mathbf{x}, \mathbf{x}_{new})$;
      else
        break;
      end
    end
    $\mathbf{E} \leftarrow (\mathbf{E} \setminus \{(\mathbf{x}, \mathbf{x}_{parent})\}) \cup \{(\mathbf{x}_{new}, \mathbf{x})\}$;
  else
    break;
  end
end

After the GO/NO-GO map is available, we can use an obstacle check function to avoid the unnecessary computational cost before solving MMR_v and MMR_a. The obstacle check passes, if there is no NO-GO area between the two nodes. The details of TRs-B-RRT* are given in Algorithm 2.

In the next section, we use a case study to demonstrate the proposed reliability-based path planning algorithm in comparison with the conventional RRT* without any reliability considerations.

V. Case Study

In this example, we use a 200×200 m target map to demonstrate the proposed path planning method. The map is obtained from the ARCGIS/ENVI database with uncertainty. High-fidelity simulation by PyChrono is used to obtain the training data for the construction of the two surrogate models. The proposed TRs-RRT* and TRs-B-RRT* are applied to find the optimal path with required reliability targets. The optimal path found is validated using PyChrono simulation. The detailed map and soil parameter information and results are provided below.

TABLE I
STATISTICAL INFORMATION OF DIFFERENT SLOPE/SOIL PARAMETERS.

Slope/Soil ID	Height		Soil Parameters											
	h (m)		k_ϕ		k_c		B_n		c (Pa)		ϕ_f (°)		J (m)	
	μ	σ	μ	σ	μ	σ	μ	σ	μ	σ	μ	σ	μ	σ
1	1.3	0.45	1×10^9	1,000	5×10^8	500	2.8	0.01	950	1	37.5	0.5	0.048	0.001
2			5×10^8	1,500	1×10^8	750	2.6	0.05	800	2.5	35.0	1.0	0.04	0.002
3			1×10^8	2,000	5×10^7	2,500	2.2	0.1	650	5	32.5	1.5	0.036	0.002
4			5×10^7	500	1×10^7	1,500	2.2	0.02	500	10	30.0	1.0	0.032	0.003
5			1×10^7	1,000	5×10^6	1,000	2.0	0.1	450	15	27.5	2.0	0.029	0.002

A. Map Information and Soil Properties

As discussed previously, uncertainty exists in the target area due to the complex surrounding environment. We use the Gaussian random field to model the uncertainty over space. A realization of the random fields (height and soil parameters) is shown in Fig. 7. Note that the map given in Fig. 7 has been artificially modified in order to demonstrate the differences between different path planning algorithms. TABLE I gives the uncertainty parameters of the target map. We assume that five different soils could exist in the target map. The properties of each soil are described using six parameters, which are Bekker coefficients (k_ϕ, k_c, B_n), soil cohesion (c), friction angle (ϕ_f), and Janosi shear displacement (J_s). All the soil parameters together with height are represented by the Gaussian random field with a correlation length of 30 m.

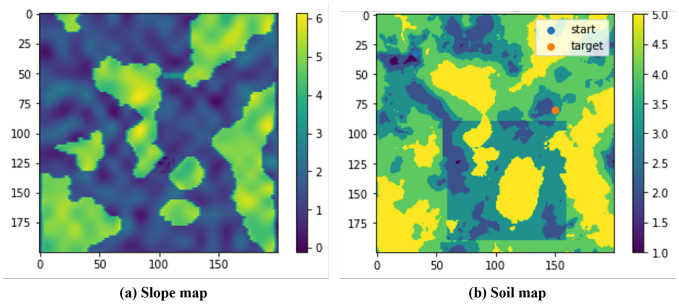

Fig. 7. Map of interest; (a) Height map and (b) Soil map.

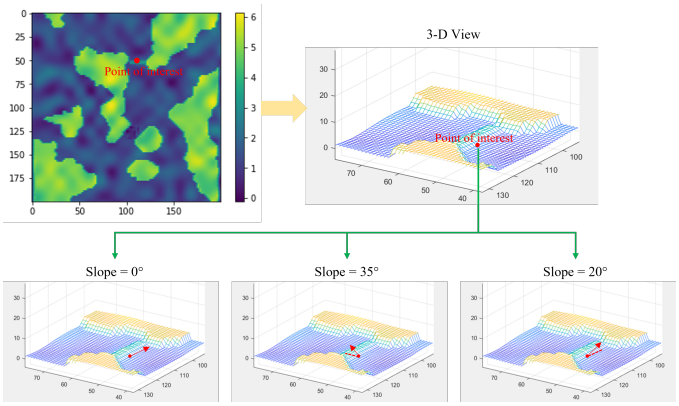

Fig. 8. Slope variation due to different moving directions.

B. Construction of Mobility Model

As discussed in Sec. III-B and Sec. III-C, we use adaptive GP and DENA as surrogate models to predict the maximum attainable speed and vertical acceleration, respectively. For adaptive GP, we use 100 initial training points from Latin Hypercube Sampling (LHS) to construct an initial GP model. Active learning then refines the GP model iteratively until satisfactory accuracy is achieved.

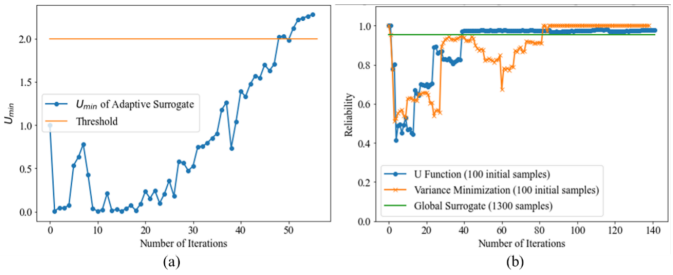

Fig. 9. The results of adaptive GP and comparison with other methods.

The convergence history and accuracy of adaptive GP are shown in Fig. 9. From Fig. 9(a), we see that after 45 iterations, the minimum value of U from Eq. (6) is larger than 2. The accuracy of adaptive GP is compared with the ground truth by Monte Carlo Simulation (MCS) and variance minimization

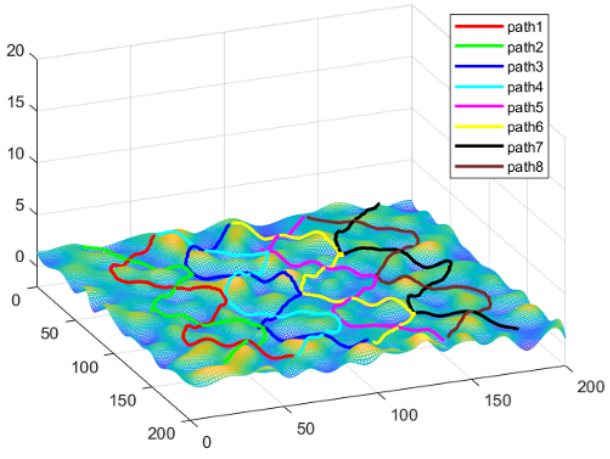

Fig. 10. The height contour and generated eight paths.

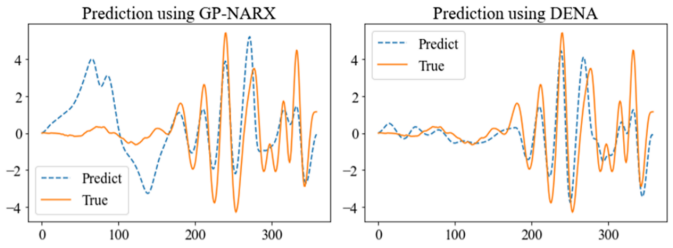

Fig. 11. Comparison between DENA and GP-NARX.

method as shown in Fig. 9(b). It shows that the active learning based adaptive GP converges faster with good accuracy.

To obtain the DENA model for vertical acceleration, we use the training data collected from a deformable terrain of the target map. The terrain is a realization of a Gaussian random field. From the realization, we generate eight paths in which the data (heights and vertical acceleration) of seven paths are used to train the DENA model, and the data from the eighth path is for test. Fig. 10 shows the 3-D terrain and paths.

Using the method discussed in Sec. III-C, the cluster number Q is determined to be two and the optimal number of lags for NARX models is identified as five. The test result of path eight is given in Fig. 11. We compared the results of DENA and GP-NARX. It shows that DENA can capture the dynamic behavior of the vertical velocity better than GP-NARX.

C. Results of Path Planning

After the surrogate models are constructed, we can obtain reliability in terms of maximum attainable speed and vertical acceleration for any given path. The RRT* and reliability constraints from surrogate models are combined for path planning.

We evaluate four different methods, which are RRT* with GO/NO-GO map (RRT*), RRT* with one reliability constraint (R-RRT*), TRs-RRT*, and TRs-B-RRT*. The same evaluation criteria are used for performance assessment, including the length of the generated path, reliability in terms of maximum attainable speed and vertical acceleration, and computation time. The reliability is evaluated using MCS with $5,000$ samples. The detailed results for different methods are provided below. Fig. 12 shows the paths obtained from different methods.

From Fig. 12, we can observe that RRT* has the shortest path as it does not consider any reliability constraints. TRs-RRT* and TRs-B-RRT* have similar paths visually. R-RRT* considers the reliability in terms of maximum attainable speed. After reliability analysis (as shown in Fig. 13), it is found that the AGV has a high chance of losing mobility if it crosses the bump as indicated in this figure. Since there is no reliability consideration in RRT*, the identified path from RRT* (i.e., Fig. 12(a)) has a high risk of failure. This is the reason why the path identified from R-RRT* (i.e., Fig. 12(b)) bypasses the bump highlighted in Fig. 13, and is longer than the path obtained from RRT* in Fig. 12(a).

In Fig. 12(c), TRs-RRT* chooses to avoid the valley as illustrated in Fig. 14, which results in a longer path. This is

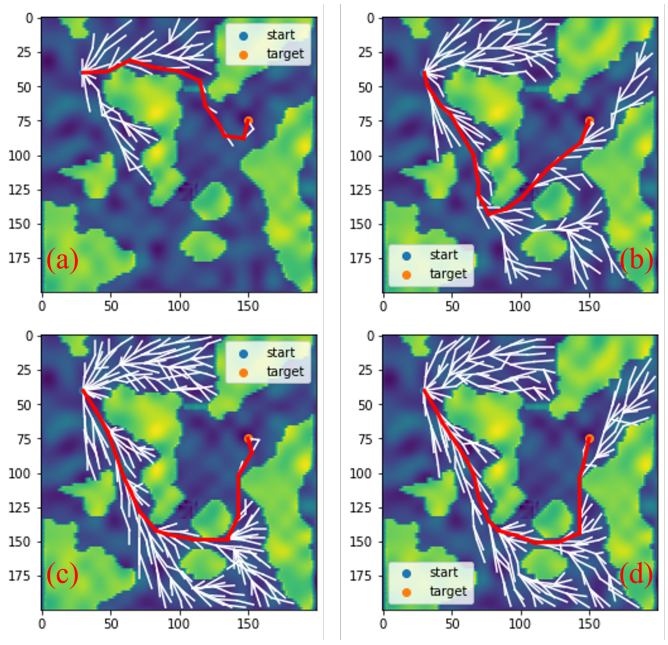

Fig. 12. Path planning by different methods; (a) RRT*; (b) R-RRT*; (c) TRs-RRT*; and (d) TRs-B-RRT*.

because TRs-RRT* has more reliability considerations than R-RRT*. As shown in Fig. 14, the terrain condition of the valley is very bumpy, which could cause high vertical accelerations of AGVs and damage the supplies or the vehicle. With more reliability considerations, TRs-RRT* (i.e., Fig. 12(c)) identifies a longer path than R-RRT* in Fig. 12(b).

To further compare different methods, MCS is used to evaluate the reliability. For illustration, we only provide the detailed simulation results of RRT*, which is shown in Fig. 15. We assume the AGV losses mobility if the speed is lowers than $2\ \mathrm{m/s}$ and the AVG or the inside supply could be damaged if the vertical acceleration exceeds $5\ \mathrm{m/s^2}$. It is obvious that the AGV fails to maintain mobility for some simulations and the AGV or the inside supply is damaged for most of the simulations. The other methods are also evaluated using the same MCS samples, but their figures are not provided due to limited space.

TABLE II gives the results of different methods quantitatively. As expected, path identified from RRT* has the lowest reliability which is consistent with the results in Fig. 15, although it has the shortest path. R-RRT* has low reliability in the vertical acceleration and it is more efficient than TRs-

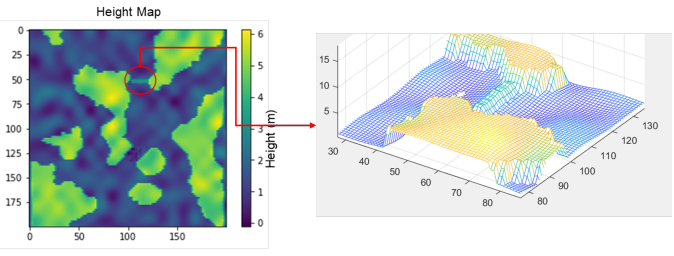

Fig. 13. Illustration of a high-risk area of mobility loss.

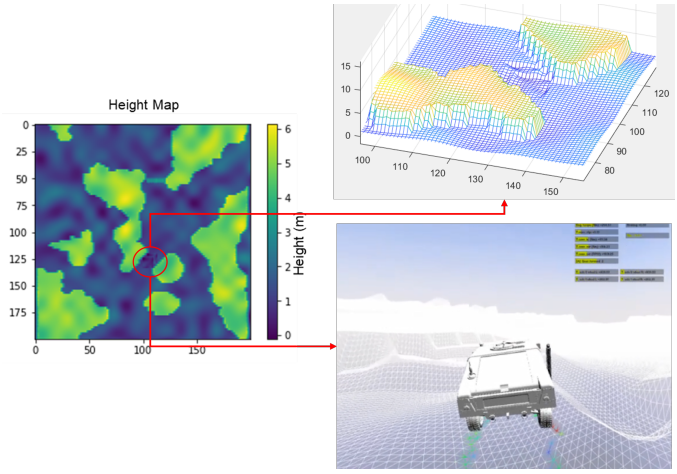

Fig. 14. Illustration of bumpy terrain condition.

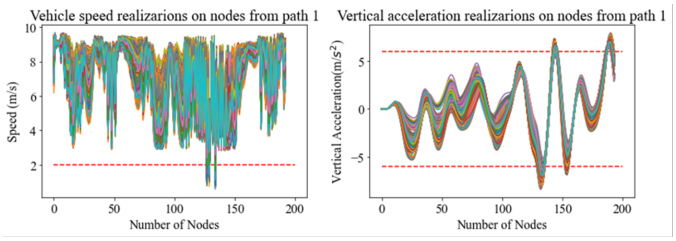

Fig. 15. The MCS results of RRT* with 5,000 samples.

TABLE II
COMPARISON OF DIFFERENT METHODS.

Method	Length of the path (m)	MMR_v	MMR_a	Computation time (h)
RRT*	146.56	0.84	0	0.15
R-RRT*	225.24	0.96	0.58	1.12
TRs-RRT*	246.71	0.99	0.98	3.37
TRs-B-RRT*	248.31	0.99	0.97	2.5

RRT* and TRs-B-RRT*. TRs-B-RRT* improves the efficiency by decreasing computation time by 1.17 hours compared with TRs-RRT* with only a bit of sacrifice in R_a. Both paths identified from TRs-RRT* and TRs-B-RRT* satisfy the reliability requirement of 0.95.

VI. CONCLUSIONS

This paper proposes a reliability-based global path planning approach for off-road autonomous vehicles (AGVs) based on the Rapidly-exploring Random Tree Star (RRT*) method while considering two reliability constraints due to prevalent uncertainty in the deformable terrain. Since the high-fidelity simulation model is computationally too expansive to use for reliability analysis, two surrogate models including an adaptative GP and a DENA-GP, are created based on the data from limited high-fidelity simulations for reliability analysis to improve the efficiency. We combine RRT* with the two reliability constraints from the surrogate models, which result in the proposed TRs-RRT* and TRs-B-RRT* path planning algorithms. The case study shows that both TRs-RRT* and TRs-B-RRT* can identify the optimal path in the map with reliability targets achieved. TRs-B-RRT* is more efficient than TRs-RRT* as the binary operation of GO/NO-GO map can avoid infeasible locations before reliability analysis.

Even though TRs-B-RRT* is computationally cheaper than TRs-RRT*, the required computational effort is too high for real-time path planning due to the consideration of reliability constraints. In addition, current simulation-based path planning method replies on physics-based computational simulations using PyChrono. The discrepancy/model-form uncertainty of PyChrono could affect the effectiveness of the proposed method [51]. In our future work, three research directions are planned, 1) to further reduce the required computational time by integrating the proposed method with advanced reliability analysis method, 2) to account for model-form uncertainty of PyChrono in path planning, and 3) to apply and validate the proposed method using field tests in the off-road environment.

ACKNOWLEDGMENTS

This work was supported in part by the Automotive Research Center (ARC) in accordance with Cooperative Agreement W56HZV-19-2-0001 U.S. Army CCDC Ground Vehicle Systems Center (GVSC), Warren, MI, and in part by the U.S. National Science Foundation under Grant CMMI-2301012. The support is gratefully acknowledged.

REFERENCES

[1] S. Ge, Y. Xie, K. Liu, Z. Ding, E. Hu, L. Chen, and F.-Y. Wang, "The use of intelligent vehicles and artificial intelligence in mining operations: Ethics, responsibility, and sustainability," *IEEE Transactions on Intelligent Vehicles*, vol. 8, no. 2, pp. 1021–1024, 2023.

[2] S. Ge, F.-Y. Wang, J. Yang, Z. Ding, X. Wang, Y. Li, S. Teng, Z. Liu, Y. Ai, and L. Chen, "Making standards for smart mining operations: Intelligent vehicles for autonomous mining transportation," *IEEE Transactions on Intelligent Vehicles*, vol. 7, no. 3, pp. 413–416, 2022.

[3] Y. Huang, S. Z. Yong, and Y. Chen, "Stability control of autonomous ground vehicles using control-dependent barrier functions," *IEEE Transactions on Intelligent Vehicles*, vol. 6, no. 4, pp. 699–710, 2021.

[4] J. E. Naranjo, M. Clavijo, F. Jiménez, O. Gomez, J. L. Rivera, and M. Anguita, "Autonomous vehicle for surveillance missions in off-road environment," in *2016 IEEE Intelligent Vehicles Symposium (IV)*. IEEE, 2016, pp. 98–103.

[5] Q. Liu, L. Zhao, Z. Tan, and W. Chen, "Global path planning for autonomous vehicles in off-road environment via an A-star algorithm," *International Journal of Vehicle Autonomous Systems*, vol. 13, no. 4, pp. 330–339, 2017.

[6] T. Oksanen and A. Visala, "Coverage path planning algorithms for agricultural field machines," *Journal of field robotics*, vol. 26, no. 8, pp. 651–668, 2009.

[7] S. LaValle, "Rapidly-exploring random trees: A new tool for path planning," *Research Report 9811*, 1998.

[8] K. Chu, M. Lee, and M. Sunwoo, "Local path planning for off-road autonomous driving with avoidance of static obstacles," *IEEE transactions on intelligent transportation systems*, vol. 13, no. 4, pp. 1599–1616, 2012.

[9] A. Gasparetto, P. Boscariol, A. Lanzutti, and R. Vidoni, "Path planning and trajectory planning algorithms: A general overview," *Motion and operation planning of robotic systems*, pp. 3–27, 2015.

[10] S. Teng, X. Hu, P. Deng, B. Li, Y. Li, Y. Ai, D. Yang, L. Li, Z. Xuanyuan, F. Zhu *et al.*, "Motion planning for autonomous driving: The state of the art and future perspectives," *IEEE Transactions on Intelligent Vehicles*, 2023.

[11] Z. Zang, J. Song, Y. Lu, X. Zhang, Y. Tan, Z. Ju, H. Dong, Y. Li, and J. Gong, "A unified framework integrating trajectory planning and motion optimization based on spatio-temporal safety corridor for multiple agvs," *IEEE Transactions on Intelligent Vehicles*, pp. 1–12, 2023.

[12] D. Zhu and S. X. Yang, "Bio-inspired neural network-based optimal path planning for UUVs under the effect of ocean currents," *IEEE Transactions on Intelligent Vehicles*, vol. 7, no. 2, pp. 231–239, 2021.

[13] A. Pal, A. Bhattacharya, and A. K. Chakraborty, "Planning of ev charging station with distribution network expansion considering traffic congestion and uncertainties," *IEEE Transactions on Industry Applications*, 2023.

[14] C. Cai and S. Ferrari, "Information-driven sensor path planning by approximate cell decomposition," *IEEE Transactions on Systems, Man, and Cybernetics, Part B (Cybernetics)*, vol. 39, no. 3, pp. 672–689, 2009.

[15] A. Yazici, G. Kirlik, O. Parlaktuna, and A. Sipahioglu, "A dynamic path planning approach for multirobot sensor-based coverage considering energy constraints," *IEEE transactions on cybernetics*, vol. 44, no. 3, pp. 305–314, 2013.

[16] N. Ayoub, M. Asad, M. Aslam, Z. Gao, E. U. Munir, and R. Tobji, "MAHEE: Multi-hop advance heterogeneity-aware energy efficient path planning algorithm for wireless sensor networks," in *2017 IEEE Pacific Rim conference on communications, computers and signal processing (PACRIM)*. IEEE, 2017, pp. 1–6.

[17] H. Ma, F. Meng, C. Ye, J. Wang, and M. Q.-H. Meng, "Bi-Risk-RRT based efficient motion planning for autonomous ground vehicles," *IEEE Transactions on Intelligent Vehicles*, vol. 7, no. 3, pp. 722–733, 2022.

[18] H. Guo, C. Shen, H. Zhang, H. Chen, and R. Jia, "Simultaneous trajectory planning and tracking using an mpc method for cyber-physical systems: A case study of obstacle avoidance for an intelligent vehicle," *IEEE Transactions on Industrial Informatics*, vol. 14, no. 9, pp. 4273–4283, 2018.

[19] C. Jiang, Z. Hu, Z. P. Mourelatos, D. Gorsich, P. Jayakumar, Y. Fu, and M. Majcher, "R2-RRT*: reliability-based robust mission planning of off-road autonomous ground vehicle under uncertain terrain environment," *IEEE Transactions on Automation Science and Engineering*, vol. 19, no. 2, pp. 1030–1046, 2021.

[20] Z. Hu, Z. P. Mourelatos, D. Gorsich, P. Jayakumar, and M. Majcher, "Testing design optimization for uncertainty reduction in generating off-road mobility map using a bayesian approach," *Journal of Mechanical Design*, vol. 142, no. 2, 2020.

[21] P. Jayakumar and D. Mechergui, "Efficient generation of accurate mobility maps using machine learning algorithms," US ARMY TARDEC WARREN United States, Tech. Rep., 2019.

[22] R. Gonzalez, P. Jayakumar, and K. Iagnemma, "Generation of stochastic mobility maps for large-scale route planning of ground vehicles: A case study," *Journal of Terramechanics*, vol. 69, pp. 1–11, 2017.

[23] M. McCullough, P. Jayakumar, J. Dasch, and D. Gorsich, "The next generation NATO reference mobility model development," *Journal of Terramechanics*, vol. 73, pp. 49–60, 2017.

[24] E. Petrick, Z. Janosi, and P. Haley, "The use of the nato reference mobility model in military vehicle procurement," SAE Technical Paper, Tech. Rep., 1981.

[25] J. Hetherington, "The applicability of the MMP concept in specifying off-road mobility for wheeled and tracked vehicles," *Journal of terramechanics*, vol. 38, no. 2, pp. 63–70, 2001.

[26] D. Rowland, "Tracked vehicle ground pressure and its effect on soft ground performance," in *Proceedings of the 4th International ISTVS Conference April*, 1972, pp. 24–28.

[27] J. Wong, "On the role of mean maximum pressure as an indicator of cross-country mobility for tracked vehicles," *Journal of terramechanics*, vol. 31, no. 3, pp. 197–213, 1994.

[28] J. Wong, P. Jayakumar, E. Toma, and J. Preston-Thomas, "A review of mobility metrics for next generation vehicle mobility models," *Journal of Terramechanics*, vol. 87, pp. 11–20, 2020.

[29] M. Bradbury, J. Dasch, R. Gonzalez, H. Hodges, A. Jain, K. Iagnemma, M. Letherwood, M. Mccullough, J. Priddy, B. Wojtysiak *et al.*, "Next-generation NATO reference mobility model (NG-NRMM)," *Tank Automotive Research, Development and Engineering Center (TARDEC), Warren, MI*, 2016.

[30] M. McCullough, P. Jayakumar, J. Dasch, and D. Gorsich, "Developing the next generation NATO reference mobility model," US ARMY TARDEC WARREN United States, Tech. Rep., 2016.

[31] K. Xia, "Finite element modeling of tire/terrain interaction: Application to predicting soil compaction and tire mobility," *Journal of Terramechanics*, vol. 48, no. 2, pp. 113–123, 2011.

[32] A. Recuero, R. Serban, B. Peterson, H. Sugiyama, P. Jayakumar, and D. Negrut, "A high-fidelity approach for vehicle mobility simulation: Nonlinear finite element tires operating on granular material," *Journal of Terramechanics*, vol. 72, pp. 39–54, 2017.

[33] R. González, P. Jayakumar, and K. Iagnemma, "Stochastic mobility prediction of ground vehicles over large spatial regions: a geostatistical approach," *Autonomous Robots*, vol. 41, no. 2, pp. 311–331, 2017.

[34] K. Choi, P. Jayakumar, M. Funk, N. Gaul, and T. M. Wasfy, "Framework of reliability-based stochastic mobility map for next generation NATO reference mobility model," *Journal of Computational and Nonlinear Dynamics*, vol. 14, no. 2, 2019.

[35] J. Yin, D. Shen, X. Du, and L. Li, "Distributed stochastic model predictive control with taguchi's robustness for vehicle platooning," *IEEE Transactions on Intelligent Transportation Systems*, 2022.

[36] D. Shen, J. Yin, X. Du, and L. Li, "Distributed nonlinear model predictive control for heterogeneous vehicle platoons under uncertainty," in *2021 IEEE International Intelligent Transportation Systems Conference (ITSC)*. IEEE, 2021, pp. 3596–3603.

[37] Y. Liu, C. Jiang, Z. P. Mourelatos, D. Gorsich, P. Jayakumar, Y. Fu, M. Majcher, and Z. Hu, "Simulation-based mission mobility reliability analysis of off-road ground vehicles," *Journal of Mechanical Design*, vol. 143, no. 3, 2021.

[38] Y. Liu, C. Jiang, X. Zhang, Z. P. Mourelatos, D. Barthlow, D. Gorsich, A. Singh, and Z. Hu, "Reliability-based multivehicle path planning under uncertainty using a bio-inspired approach," *Journal of Mechanical Design*, vol. 144, no. 9, p. 091701, 2022.

[39] S. M. LaValle and J. J. Kuffner Jr, "Randomized kinodynamic planning," *The international journal of robotics research*, vol. 20, no. 5, pp. 378–400, 2001.

[40] M. W. Achtelik, S. Weiss, M. Chli, and R. Siegwart, "Path planning for motion dependent state estimation on micro aerial vehicles," in *2013 IEEE international conference on robotics and automation*. IEEE, 2013, pp. 3926–3932.

[41] N. A. Melchior and R. Simmons, "Particle RRT for path planning with uncertainty," in *Proceedings 2007 IEEE International Conference on Robotics and Automation*. IEEE, 2007, pp. 1617–1624.

[42] I. Noreen, A. Khan, and Z. Habib, "Optimal path planning using RRT* based approaches: a survey and future directions," *International Journal of Advanced Computer Science and Applications*, vol. 7, no. 11, 2016.

[43] J. Yin, Z. Hu, Z. P. Mourelatos, D. Gorsich, A. Singh, and S. Tau, "Efficient reliability-based path planning of off-road autonomous ground vehicles through the coupling of surrogate modeling and rrt*," *IEEE Transactions on Intelligent Transportation Systems*, pp. 1–16, 2023.

[44] J. Yin and X. Du, "High-dimensional reliability method accounting for important and unimportant input variables," *Journal of Mechanical Design*, vol. 144, no. 4, 2022.

[45] A. Gallina, R. Krenn, M. Scharringhausen, T. Uhl, and B. Schäfer, "Parameter identification of a planetary rover wheel–soil contact model via a bayesian approach," *Journal of Field Robotics*, vol. 31, no. 1, pp. 161–175, 2014.

[46] R. Serban, M. Taylor, D. Negrut, and A. Tasora, "Chrono:: Vehicle: template-based ground vehicle modelling and simulation," *International Journal of Vehicle Performance*, vol. 5, no. 1, pp. 18–39, 2019.

[47] A. Tasora, R. Serban, H. Mazhar, A. Pazouki, D. Melanz, J. Fleischmann, M. Taylor, H. Sugiyama, and D. Negrut, "Chrono: an open source multi-physics dynamics engine," in *International Conference on High Performance Computing in Science and Engineering*. Springer, 2015, pp. 19–49.

[48] J. Yin and X. Du, "Active learning with generalized sliced inverse regression for high-dimensional reliability analysis," *Structural Safety*, vol. 94, p. 102151, 2022.

[49] Y. Liu, D. Barthlow, Z. P. Mourelatos, J. Zeng, D. Gorsich, A. Singh, and Z. Hu, "Mobility prediction of off-road ground vehicles using a dynamic ensemble of NARX models," *Journal of Mechanical Design*, vol. 144, no. 9, p. 091709, 2022.

[50] G. J. McLachlan and K. E. Basford, *Mixture models: Inference and applications to clustering*. M. Dekker New York, 1988, vol. 38.

[51] C. Jiang, Z. Hu, Y. Liu, Z. P. Mourelatos, D. Gorsich, and P. Jayakumar, "A sequential calibration and validation framework for model uncertainty quantification and reduction," *Computer Methods in Applied Mechanics and Engineering*, vol. 368, p. 113172, 2020.

Jianhua Yin (Member) received the B.E. and M.S. degree in Geotechnical Engineering from Chang'an University (2014), Xi'an and Nanjing University (2017), Nanjing, respectively, in China. He received the Ph.D. degree in School of Mechanical Engineering, Purdue University, West Lafayette, in 2022. He is currently a research fellow at the University of Michigan. His current research interests include uncertainty quantification, machine learning, and intelligent vehicles & transportation.

Lingxi Li (Senior Member) received his Ph.D. degree in Electrical and Computer Engineering from the University of Illinois at Urbana-Champaign in 2008. Since August 2008, he has been with Indiana University-Purdue University Indianapolis (IUPUI) where he is currently professor in electrical and computer engineering. Dr. Li's current research focuses on the modeling, analysis, control, and optimization of complex systems, intelligent transportation systems, connected and automated vehicles, active safety systems, human-machine interaction, digital twins and parallel intelligence. He has authored/co-authored over one book and 130+ research articles in refereed journals and conferences, and received two U.S. patents. Dr. Li received a number of awards including five conference best paper awards, 2021 IEEE ITSS Outstanding Application Award, 2017 Outstanding Research Contributions Award, 2012 T-ITS Outstanding Editorial Service award, and several university research/teaching awards. He is currently serving as an associate editor for five international journals.

Zissimos P. Mourelatos is currently a Distinguished Professor of Mechanical Engineering at Oakland University. He has served as the Chair of the Mechanical Engineering Department (2010-2014), and the John F. Dodge Chair of Engineering (2012-2016) at Oakland University. Before joining Oakland University, he spent 18 years at the General Motors Research and Development Center. He received his Ph.D. from the University of Michigan in 1985. Dr. Mourelatos conducts research in the areas of design under uncertainty, Reliability-Based Design Optimization, vibrations and dynamics. Dr. Mourelatos has published over 240 journal and conference publications. Dr. Mourelatos is a Fellow of ASME and SAE.

Yixuan Liu received B.E. degree in energy and power system engineering from Xi'an Jiao Tong University, Xi'an, China, in 2016, Master's degree in mechanical engineering from University of Michigan-Dearborn, Dearborn, Michigan, USA, in 2017, and Ph.D. degree in industrial and system engineering from University of Michigan-Dearborn, Dearborn, Michigan, USA, in 2022. His current research interests include vehicle simulation and modeling, vehicle mobility reliability analysis, uncertainty quantification, and machine learning.

David Gorsich is the Army's Chief Scientist of U.S. Army Combat Capabilities Development Command (CCDC) Ground Vehicle Systems Center (GVSC). He received his Ph.D. in applied mathematics from MIT. His current research interests are vehicle dynamics and structural analysis, reliability based design optimization, underbody blast modeling, terrain modeling and spatial statistics. Dr. Gorsich has published more than 150 conference and journal articles. Dr.Gorsich was named a SAE Fellow in 2008 and a ASME Fellow in 2020. He has served on the SAE Technical Standards Board, been the chair for the SAE International Standards Committee for Ground Vehicle Reliability and also on the SAE Board of Directors.

Amandeep Singh is the Branch Chief at US Army, GVSC Vehicle Dynamics and Mobility M&S team. He has over twenty-seven years of technical leadership and research experience in vehicle dynamics, mobility, and reliability working at Government and automotive industry. He received his MS from Clemson University in 1995, and PhD from Oakland University, Michigan in 2010, both in Mechanical Engineering. He is a registered Professional Engineer with the State of Michigan.

Seth Tau is a Mechanical Engineer at the U.S. Army Combat Capabilities Development Command (DEVCOM) Ground Vehicle Systems Center (GVSC). He received his Master's degree in mechanical engineering, in 2019, and his Ph.D. in mechanical engineering, in 2021, both from The Pennsylvania State University. His current research interests include vehicle dynamics and mobility, autonomous vehicle planning algorithms, machine learning, and uncertainty quantification.

Zhen Hu received B.E. degree in mechanical engineering from Central South University, Changsha, China, in 2008, Master's degree in mechatronics engineering from Huazhong University of Science and Technology, Wuhan, China, in 2011, and Ph.D. degree in mechanical engineering from Missouri University of Science and Technology, Rolla, MO, USA, in 2014. His current research interests include vehicle mobility reliability analysis, design under uncertainty, uncertainty quantification, Bayesian inference, and additive manufacturing.